SEA ICE INVESTIGATIONS FROM SEASAT TO THE PRESENT, WITH AN EMPHASIS ON ICE MOTION: WHAT HAVE WE LEARNED AND WHAT AWAITS

Benjamin Holt [1] and Ron Kwok [2]

[1] Jet Propulsion Laboratory, California Institute of Technology, Pasadena CA, 91109,USA, Email:Ben.Holt@jpl.nasa.gov

[2] Jet Propulsion Laboratory, California Institute of Technology, Pasadena CA, 91109,USA, Email:Ron.Kwok@jpl.nasa.gov

ABSTRACT

NASA launched Seasat in June 1978 carrying a remarkable array of microwave instruments designed to observe the global oceans, including an active microwave altimeter, scatterometer, and SAR along with a passive microwave radiometer. While the satellite mission ended abruptly in mid-October 1978 after only about 100 days of operation, a unique and comprehensive view of the oceans was obtained that clearly showed the extraordinary scientific value of the instruments by improving the knowledge of the oceans circulation, wind and wave field, and characterization of key aspects of the cryosphere. Aside from optical and thermal sensor data, this data set from 25 years ago essentially set the stage, providing a legacy if you will, for most of the major dedicated ocean satellite missions that have taken place since and are planned for the near future.

In this paper, we provide a short review of sea ice investigations starting from Seasat. We focus particularly on the detailed and quantitative measurements of the sea ice motion field, which were some of the earliest results from Seasat and have subsequently been shown to be of critical value to the derivation of several key climatically important variables. Other key investigations discussed include examination of the seasonal melt cycle, ice extent and concentration, and estimates of thickness from the proxy measurements of ice type and age and more directly from freeboard. We end with a brief discussion on how these measurements might be improved in the future.

1. SEA ICE AND CLIMATE

Sea ice plays a key role in Earth's climate and has long been thought to be a primary candidate as an indicator of global warming, of particular value since the polar regions are projected by global climate models to undergo the largest greenhouse warming (e.g. Kattenberg et al., 1996). Sea ice acts to reduce the flux of heat from the comparatively warm ocean to the colder atmosphere. When open water appears as the ice cover moves and deforms, the heat flux increases tenfold, which then gradually decreases as new ice forms and thickens. During ice formation, salt is released from the water crystalization process to form brine, which eventually drains out of the ice into the upper ocean. Rapid ice growth and subsequent salt rejection may result in locally dense water that mixes downward into the ocean column until it reaches its equilibrium depth. In fact, the dense water formed within areas of intense ice growth contributes significantly to the deepest waters of the world's oceans. The nearly salt-free sea ice is gradually transported equatorward by ocean currents and winds to eventually melt, putting freshwater back into the ocean at another location from initial formation, and impacting ocean vertical mixing. The final key interaction is that sea ice has a high albedo during winter that effectively reflects incoming heat back to the atmosphere. Albedo is sharply reduced when summer melt takes place, with absorption of shortwave radiation increasing with the presence of liquid water particularly within surface melt ponds. Each of these interactions will be impacted by climatic shifts in atmospheric and ocean circulation, temperature fluxes, and the length of summer melt. The interactions themselves may also accelerate or retard the impacts, thus forming feedback loops.

Recent observations strongly indicate significant climatic changes in sea ice are taking place, particularly within the Arctic. The Arctic sea ice cover was found to have thinned by over 40% between 1958-1976 and 1993-1997 as measured by submarine-mounted upward-looking sonar (Rothrock et al., 1999; 2003). The Arctic ice cover has decreased in both the maximum (Parkinson and Cavalieri, 2002) and minimum (Comiso, 2002) extent since the late 1980s. The length of the Arctic melt season appears to be increasing (Smith, 1998), which combined with the decrease in minimum extent, suggests lengthening periods of low albedo and increased heating of the extended areas of open ocean, which most likely will delay and thus reduce sea ice growth during the following winter. Hydrographic data from recent submarine and icebreaker cruises reveal large-scale changes in the structure of the Arctic upper ocean (Steele and Boyd, 1998; Bjork et al., 2002). Some of the above changes appear to be highly correlated with the North Atlantic Oscillation (NAO) and related Arctic Oscillation (AO), which are indexes of sea level pressure anomalies in the Northern Hemisphere (Proshutinsky and Johnson, 1997; Steele and Boyd, 1998). These patterns strongly affect the dominant pressure fields in the Arctic and thus both the upper ocean and ice circulation. During the late 1980's through the late 1990's, the NAO/AO index remained positive, which resulted in a weakening of the Beaufort Sea cyclonic gyre and an increase in ice transport across the Arctic and out through the Fram Strait into the North Atlantic (Kwok and Rothrock, 1999; Kwok, 2000). This pattern is thought to have reduced the overall longevity of sea ice within the Arctic and thus the thinning in mean thickness and related volume as measured by submarine sonar data.

From this simplistic view of the key sea ice interactions and the recent changes taking place, the primary geophysical measurements needed to monitor the state of the sea ice cover include thickness distribution, extent, amount of open water, albedo, and motion. The broad, synoptic view is best done with satellites and microwave sensors to provide the all-weather year round vantage point. The Seasat instrument suite was the first test of four complementary microwave sensors to provide these measurements. Some of the key measurements are made directly while others, particularly thickness, have proven to be more elusive and thus have been largely measured indirectly.

2. SEASAT INSTRUMENTS

The Seasat instruments were designed to return the maximum information from the ocean surface, including sea ice in the polar oceans. The Radar Altimeter (ALT) carefully measured the spacecraft altitude above the ocean surface, which provided wave height and sea surface height. The altimeter operated at Ku-band (13.5 GHz) and had a 10 cm vertical accuracy. The Seasat-A Satellite Scatterometer (SASS) was used to measure wind speed and direction and also backscatter over ice surfaces. The SASS operated at Ku-band (14.6 GHz) and provided wind speed accurate to +/- 2 m/s and 20 deg. in direction. The Scanning Multichannel Microwave Radiometer (SMMR) was used to measure surface wind speed (+/- 2 m/s), ocean surface temperature (+/- 2 deg C), atmospheric water vapor content, rain rate, and ice coverage. The SMMR operated at 6.6, 18, 37, 10.7 and 21 GHz with a 600 km swath width. The first passive microwave radiometer (Electroncially Scanning Microwave Radiometer or ESMR) was flown in 1973 and an identical SMMR launched on Nimbus 7 in November 1978, just after the Seasat mission. The Synthetic Aperture Radar (SAR) was used to image the ocean surface (wave patterns), polar ice, and coastal regions. The SAR operated at L-band (1.275 GHz), at a single polarization of horizontal transmit-horizontal receive (HH) with a fixed 100 km swath with incidence angles of 20-26° and a resolution of 25 m. The National Oceanic and Atmospheric Administration (NOAA) provided a fifth instrument to the Seasat Mission, a visible and infrared radiometer (VIRR), from their weather satellite program to provide surface mapping that could be compared to the data from the radar sensors.

Seasat was launched on June 26, 1978, from Vandenberg Air Force Base, California, into a near-circular polar orbit at an altitude of about 800 km and an inclination of 108°. The mission ended suddenly on October 10, 1978 due to a failure of the vehicle's electric power system. Although Seasat operated for only about 100 days, the mission not only demonstrated the feasibility of using microwave sensors to monitor ocean and sea ice conditions, but also laid the groundwork for many future missions. Evans et al. (2003) has recently summarized the legacy instrumentation and geophysical measurements accomplished since Seasat.

3. SEA ICE MEASUREMENTS

We discuss four primary sea ice measurements from microwave spaceborne sensors: ice motion, ice extent and concentration, the seasonal melt cycle, and ice thickness.

3.1.A Ice Motion

The motion of sea ice provides critical information on the ice cover over several scales. On scales larger than several hundred kilometers, the general circulation of the ice cover provides the advective component of the ice mass balance as well as a velocity boundary condition on the ocean surface. On smaller scales of kilometers, motion fields show the detailed motion of individual floes, how ice floes move as aggregates, the opening of leads, and the ridging processes. Ice motion controls the abundance of thin ice and therefore the intensive heat flux from the ocean to the atmosphere, ice production, and salinity flux. Accurate measurements of ice motion on a continuous basis over a broad region can be used in other key derivations.

Seasat SAR provided the first extensive fine resolution radar images of the western Arctic sea ice, enhanced by the 'collapse' of orbits in the polar regions which improves temporal sampling. The imagery was used to make the most detailed sea ice motion maps ever produced at the time, from which openings and closing of the ice cover clearly revealed where the largest heat exchange from the ocean to the air takes place. The identification of individual floes between images separated by a few days in time enabled the unambiguous tracking of the ice field within the central pack ((Hall and Rothrock, 1981; Curlander et al., 1985), where a deformation grid showed areas of motion and no motion (Figure 1) (Fily and Rothrock, 1987), and at the ice margins, where free drift is present and the motion field can be significantly impacted by wind and upper ocean forcing (Figure 2) (Carsey and Holt, 1987).

The Seasat SAR ice motion maps generated considerable interest, sufficient to form the basis of the scientific rationale for NASA to support the development of the Alaska SAR Facility in Fairbanks, Alaska to receive ERS-1 SAR imagery of the Arctic. There was a related flurry of activity to develop satisfactory image processing algorithms, which could efficiently capture the dynamic ice motion fields under the also varying ice conditions and radar signatures. This led to the development of the first geophysical SAR product generation system, designed to automatically produce ice motion maps from ERS-1 SAR imagery (Kwok et al., 1990). Also included in this system was identification of sea ice types, more readily identified with C-band data than on Seasat's L-band data, which is a proxy for sea ice thickness (Kwok et al., 1992). While the ice cover sampling with ERS-1 SAR was still piecemeal rather than broad, the value of these products was considerable (Fetterer et al., 1994; Stern et al., 1995).

3.1.B. RADARSAT Geophysical Processor System

The experience gained from the first geophysical algorithm development led to the next generation of motion observations produced with the wide swath capability of RADARSAT-1, called the RADARSAT Geophysical Processor System (RGPS) (Kwok, 1998). RADARSAT-1 provided complete coverage maps of the entire Arctic Ocean repeated every 3-6 days, which in fact have been continuously obtained since October 1996. Included in this second generation product system was the addition of a very significant tracking enhancement, going from Eulerian tracking (tracking floes from image A to image B and then resetting the grid to track from image B to image C) employed in the first product development (Kwok et al., 1990) to Lagrangian tracking (Kwok et al., 1995). By tracking a grid element (cell) continuously over time, not only could the trajectory and detailed deformation of that element be observed, but the age of any newly formed ice as well as loss of ice area to ridging could be derived as well. This age tracking has been used to derive first year ice thickness over entire winter seasons, thereby accounting for a major component of the mass balance of sea ice, which has been found to vary annually and in relation to the overall transport of ice within and out of the Arctic (Kwok and Cunningham, 2002).

The following provides a brief description of the RGPS approach used in estimating ice age and thickness from the time-varying cell deformations derived from ice motion. An age histogram of sea ice specifies the fractional area covered by ice of different chronological ages. The construction of such a histogram involves the steps below. At each time step, positive area changes are

interpreted as the creation of areas of open water. New ice is assumed to grow over these areas immediately after opening. For this ice, a new age category in the histogram is introduced. At the same time, pre-existing age categories in the histogram are 'aged' by the length of the time step. A decrease in cell area is assumed to have ridged the youngest ice in the cell, reducing its area. The assumption here is that once ridging starts, the deformation tends to be localized in the recently formed thinner and weaker ice in leads. This area of ridged ice is tracked as a separate category in the age histogram. In Figure 3, this procedure created five age categories from the sequence of positive area changes since Day 335. Ice age is converted to ice thickness using an empirical ice growth formula. The growth rate is approximated using Lebedev's parameterization, which depends on the number of freezing-degree days. Volume is conserved and ridged ice is assumed to be five times its original thickness and occupies a quarter of the area [Parmerter and Coon, 1972]. The dataset provides fine age/thickness resolution of only the young/thin end of the age/thickness distributions, but this is the crucial range that produces the most ice growth, the most turbulent heat flux to the atmosphere and the most salt flux to the ocean.

For a given winter, typically 30,000 grid cells with initial dimensions of 10 km on a side are used to sample the motion and deformation of the ice cover. Effectively, this is identical to deploying the same number of drifting buoys. Figure 4 shows a basin-scale view of the divergence, vorticity, and shear of the ice cover sampled by the RGPS cells. The deformation fields show linear kinematic features (LKFs) that characterize the opening, closing, and shear of the ice cover. These high-resolution ice motion from the RGPS, with data quality comparable to that from buoy drifts (~0.1 cm/s) [Lindsay and Stern, 2003], have provided an unprecedented level of spatial and temporal detail of deformational features. For the first time, we can map on a routine basis the location, coverage, and seasonal development of leads and ridges. The RGPS data have shown that narrow fracture zones (up to kilometers wide) are long linear features that can extend for thousands of kilometers and these fracture patterns appear as oriented rather than random patterns from the kilometer scale to the scale of the Arctic basin (Figure 4). With the advent of high-resolution coupled ice-ocean models (10 km) that approaches the widths of leads, there is an increased need for high-resolution measurements for validation of model results [e.g. Zhang et al., 2003]. Simulation and model performance can now be examined in detail using the small-scale RGPS observations previously unavailable [Hibler, 2001; Richter-Menge et al., 2002].

As of this writing, the RGPS has produced ~4 years of sea ice observations of the Arctic Ocean. Extensive measurements of the ice motion can be used in concert with a variety of ice models for verification studies, for driving the models as forcing fields, and in data assimilation procedures. The ice production rates estimated with RGPS can be compared to those computed by models driven by the geostrophic wind and a force balance approach. The ice motion measured with RGPS can be used directly as a forcing field for an ice model and the uncertainty in the ice motion can thus be reduced. Finally, the RGPS ice displacement measurements can be assimilated directly into an ice/ocean model so that ice trajectories in the model can be made to match the observed trajectories. The value of these uses for the RGPS products will increase as the observational record becomes longer and a greater variety of seasons are recorded. The preliminary results for four winter seasons have seen that ice cover evolved in markedly different manners. Ultimately, a long record of the ice deformation and ice production rates can be developed that will contribute to the assessment of the evolution of the Arctic Ocean.

3.1.C Lower resolution ice motion fields

Ice motion fields also have been produced from a variety of lower resolution sensors. It has been demonstrated [Agnew et al., 1997; Emery et al., 1997; Liu and Cavalieri, 1998; Kwok et al., 1998] that despite antenna footprints of ten or more kilometers, data from low-resolution passive microwave radiometers and scatterometers can provide rather coarse measurements of ice motion. The combination of daily ice motion from the 85 GHz channel of SSM/I and 2-day ice motion from the 37 GHz channel of SMMR, has provided an ice motion data record dating back to 1978. The quality of the scatterometer motion fields (~5 km uncertainty in displacement), obtained from NSCAT and QuikSCAT (Liu et al., 1999) are comparable to that derived from the 85 GHz SSM/I data. The daily ice motion measurements from QuikSCAT seem complementary to the passive microwave observations. The relative merits of the scatterometer versus the passive microwave ice motion remain to be examined. Summer ice motion from scatterometers and radiometers are unreliable due to surface melt and in the case of passive microwave data, the added contamination by increased atmospheric water content with increasing temperature. With the level of uncertainty from these low resolution data, these measurements are more suited to the study of large-scale circulation patterns [Emery et al., 1997; Kwok, 2000] and ice export [Kwok and Rothrock, 1999; Martin and Augstein, 2000], rather than the small-scale processes associated with openings and closings of the ice cover.

Sequential AVHRR imagery provides moderate resolution ice motion from its visible, near-infrared, and thermal infrared bands with uncertainties of 1 km and 5 km, depending on the data products. The thermal bands can be used in winter darkness. The only drawback is that clouds obscure the surface, moderately during the winter and quite substantially during the summer. An ice motion data set dating back to 1982 is available at the National Snow and Ice Data Center in Boulder, Colorado.

3.2 Ice extent and concentration

The extent of the sea ice cover is highly correlated with air temperature, since ice will only form when the ocean temperatures have been sufficiently cooled to the freezing point by overlying air temperatures. Ice concentration provides an estimate of the percent of open water and ice within the ice cover, which can provide an indication of the heat fluxes and ice production. The multichannel combinations of the spaceborne passive microwave (PM) radiometers are sensitive to open water and ice, which combined with the all- weather, broad daily coverage of the polar regions, results in PM being a primary observational sensor for ice extent and concentration.

The ice extent measurements from these sensors provide the longest continuous time series of sea ice observations available, dating back to 1978, and have been extensively used to examine climatic trends. As mentioned before, the Arctic has undergone considerable recent retreat in ice extent (e.g. Parkinson and Cavalieri, 2002; Comiso, 2002) while the Antarctic sea ice cover has shown a slight increase in extent (Zwally et al., 2002A). The impact of the Seasat SMMR data was not critical to the

development of this time series but did verify the value of these measurements, but the companion SMMR launched later in 1978 was critical. Recent studies have examined possible improvements to ice edge detection with higher resolution data, including from the recently launched AMSR sensors, and also from other sensors including the scatterometers on NSCAT and QuikScat, and the wide swath SAR on RADARSAT (Yueh et al., 1997; Remund et al., 2000).

3.3 Seasonal cycle

With the onset of sea ice melt, surface albedo is reduced allowing more absorption of shortwave radiation. The open ocean adjacent to the sea ice also is warmed, enhancing lateral ice melt. When the air temperatures cool below freezing in fall, the switch is reversed, signalling the increase in albedo and the end of significant freshwater input from sea ice to the ocean. Soon after the end of melt, the surrounding water will eventually cool to freezing when ice formation is initiated. The duration of the melt season and the resulting open water play important roles in the overall sea ice mass balance (e.g. Zhang et al., 2000). Albedo is a difficult measurement to obtain, as it is impacted by ice type, snow cover, temperature, ice concentration and cloud cover, which by themselves are difficult to measure in summer. The seasonal melt cycle is detectable by both active and passive microwave sensors, which provide a method of capturing melt duration or the effective period of reduced albedo.

Both the SASS and SMMR were found to be sensitive to the presence of liquid water (Carsey, 1985). Melt onset is commonly a rather sharp transition when the snow and ice surfaces become wet, which results in a sharp reduction in backscatter and an increase in brightness temperature (Figure 5). During mid-summer, the surface conditions can vary rapidly as melt ponds expand and then drain and as air temperatures cycle rapidly above and below freezing. Freeze-up is usually considered as the end of surface melt, where the above trends in brightness temperatures and backscatter reverse. Freeze-up tends to be more gradual, however, and the responses can rapidly vary until settling into characteristic winter-like sea ice signatures (Winebrenner et al., 1998).

Most time-series studies of sea ice seasonal transitions in the Arctic focus on melt onset using PM (Drobot and Anderson, 2001). A correlation between varying melt onset dates has been found with the AO index, indicating the sensitivity of this signal to air temperature (Drobot and Anderson, 2001). A combined sensor analysis using SMMI and NSCAT has shown substantial differences in the date of melt onset (Forster et al., 2001). Combining RADARSAT and SMMI, substantial variation during the seasonal cycle was related to the extent of melt ponding and new ice formation after freeze-up (Comiso and Kwok, 1996). Scatterometer seasonal cycles have also been examined in the Antarctic using scatterometer data from ERS and NSCAT (Drinkwater and Liu, 2000). The single time series study, using both SMMR and SSMI, where both seasonal transitions were detected showed an apparent increase in the duration of the melt season had occurred between 1978-1996 (Smith, 1998).

3.4 Ice thickness and its proxy measurements

Ice thickness is the fundamentally single most important sea ice measurement, having been discussed as the 'great integrator' of polar climate, because thickness responds to fluxes and forcings in both the atmosphere and ocean. Thickness is thought to be the primary indicator of global greenhouse warming, yet it has proven to be one of the most difficult variables to measure particularly on meaningful synoptic and climatic scales including from satellites (U. S. National Research Council, 2001). The most comprehensive thickness measurements have been obtained from upward-looking sonar data mounted on submarines or moorings where observations extend back to the 1950's. The submarine-based results provide synoptic but highly irregular ice draft measurements over the central pack ice dating back to the 1950s, but until recently these data were classified and difficult to access. Fortuitously, in the early 1990's the US Navy made submarine cruises available for scientific exploitation, which also helped make data from earlier cruises more accessible for analysis and publication. From these data, Rothrock et al. (1999) found a decrease in mean sea ice draft— portion of ice below the ocean surface— from 3.1 m in 1958-1976 to 1.8 m in 1993-1997.

From a remote sensor, there are several approaches that may be taken to measure thickness. One approach is to measure freeboard, the portion of the ice cover above sea level. This requires highly accurate measurement of absolute height since freeboard is approximately 10% of the entire sea ice thickness volume, the identification of open water to correct for freeboard, and some knowledge of the overlying snow cover. Here both laser and radar altimeters provide important approaches. Another possible approach is the direct detection of both the ice surface- and bottom-sides. This requires lower than normal spaceborne radar frequencies (less than 1 GHz) to overcome the lossy nature of sea ice and to penetrate to many meters of thickness. However, as the frequencies less than 1 GHz allocated for scientific research are quite limited, innovative techniques are required to make use of the limited bandwidth to obtain satisfactory vertical resolution. The use of electromagnetic induction (frequencies of tens of Hz) has become a standard in situ device but these measurements have reduced accuracy with increasing height off the ice surface and over thick ice. Low frequency impulse radars have been tested with mixed results (Kovacs and Morey, 1986). More commonly, proxy indicators of thickness have been identified, specifically ice type, and more recently ice age via the RGPS lagrangian approach, using microwave brightness temperature, surface temperature obtained with near infrared and thermal imagers, and radar backscatter derived with synthetic aperture radars and scatterometers. Various combinations of channels are sensitive to the primary ice types – thin and thick first-year, multiyear ice, and the rapidly varying new and young ice.

All the Seasat instruments were evaluated for ice type to some level (Carsey, 1985; Carsey and Pihos, 1989) including the use of altimeter waveforms (Ulander, 1987). Usually these results were less than satisfying, even using image-processing algorithms. With ERS-1, it was found that C-band (both SAR and scatterometer) provided much better discrimination between multiyear and first-year ice, with still some confusion between young ice and multiyear ice (Kwok et al., 1992; Fetterer et al., 1994). The wide swath of the C-band RADARSAT data led to significant improvements in ice typing for ice charts developed by the US and foreign ice centers (Bertoia et al., 1998). As indicated by the Seasat SASS results, the 13-14 GHz frequencies of NSCAT and QuikScat enable the clear separation of the perennial and seasonal ice zones, which are currently being developed as a climatically valuable dataset over the Arctic (Kwok and Cunningham, 2002). Lastly, as mentioned previously in the

RGPS section, the use of Lagrangian tracking led to the ability to measure ice age (based on initial date of ice formation) (Figure 4). This key step jumped over the confusion in ice type measurement accuracy by deriving the even more valuable measurement of ice age. Using a simple algorithm based on freezing-degree days, estimates of thin ice thickness and loss in area to ridging were also generated, from which estimates of first-year ice production have been derived (Kwok et al., 1999; Kwok and Cunningham, 2002).

The Seasat altimeter, based on careful analysis of the waveforms, was used to measure the elevation of polar ice sheets of Greenland and Antarctic, specifically to estimate mass balance and slope changes in ice shelves (Zwally et al., 2002B). Improvements in the waveform tracking over land were made on the ERS-1/2 altimeters, leading to time series studies of elevation change (Wingham et al., 1998; Zwally et al., 2002B).

It was pointed out by Laxon [1994] that height deflections associated with diffuse echoes over ice-covered seas could be used to estimate ice freeboard. The first example of ice freeboard measurements is given in Peacock et al. [1998]. Since only 10% of the floating ice is above the ocean surface, freeboard measurement errors are magnified when applied to estimating ice thickness. Comparisons of altimetric ice thickness estimates with observations of ice draft from moored and submarine give an estimate of the uncertainty in the retrieved ice thickness of approximately 0.5 m. Figure 6 shows an example of a gridded (100 km) field of altimeter ice thickness derived from the ERS-2 radar altimeter. The radar altimeter measurements address the mean ice thickness over length scales of perhaps 100 km.

There are still a number of difficulties associated with understanding the achievable accuracy of the freeboard measurement. Some examples include the possible height biases introduced by the snow layer and the dependence of the height measurement on the location of the scattering center (snow-ice boundary or within the snow layer). Another issue is the variability in the estimates due to ice advection and deformation since height estimates within a grid cell are taken from measurements obtained over a month. Nevertheless, this technique represents a significant advancement in the measurement of sea ice thickness. The impact of this method for climate and sea ice studies would be enormous if continual long-term direct observations of ice freeboard and thence ice thickness can be realized.

Just recently, sea ice freeboard measurements from ERS-1 and ERS-2 have shown a high-frequency interannual variability in mean ice thickness that the authors suggest is related to summer melt rather than circulation (Laxon et al., 2003). Such freeboard studies are expected to continue with NASA's laser altimeter on the ICESAT mission launched in early 2003, the ENVISAT altimeter launched in 2002, and ESA's upcoming CRYOSAT radar altimeter mission to be launched in 2004 (Wingham, 1999).

4. DISCUSSION AND FUTURE ASSESSMENTS

We have attempted to briefly illustrate the value of the initial suite of Seasat microwave instruments for sea ice studies and how following missions and sensors have led to the development of critical time series to assess the climatically changing polar regions. Now we provide considerations on how these measurements might be improved in the future.

The RGPS basin-scale products of sea ice age and thickness are truly unique and we anticipate that these data products will have important utility for use in comparisons with climate models and other sensors and data sets. Also, the Arctic is undergoing measurable change this decade in several key indicators of climate warming. The to-date 4-year time record from RADARSAT is fortuitously timed to also potentially provide indicators of climate change through ice motion and age/thickness derivations, which are used to determine the surface heat and mass balance of the Arctic Ocean. It therefore seems both desirable and justifiable to continue the unique RGPS derivations over an extended time period. The ENVISAT ASAR wide swath mode presents an excellent opportunity for continued acquisition of high-resolution SAR mapping of the Arctic Ocean. Here we present a brief description of the RGPS requirements and the utility of the ENVISAT ASAR imagery.

In terms of general SAR requirements for the RGPS, repeat wide-swath SAR surveys of the entire Arctic at preferably 3-day near repeat sub-cycles are needed to determine the motion field of the ice cover. Resolution on the order of 100-200 m will resolve moderate deformation and opening/closing of important size-scale of leads. From these, ice age and thickness can be derived over comparatively short time periods. Relative radiometric accuracy of 1 dB or less across the swath provides adequate stability needed for maintaining high areal correlation of ice features between successive images. Geometric location of 300 m or better is needed to reduce feature-tracking errors. For frequency, C-band SAR is preferred due to the high radar contrast between first-year, multiyear, and wind-roughened open water, which improves feature tracking. One caveat is that the Lagrangian tracking approach used to obtain ice age places high demand on successful and regular repeating mappings. If an 'ice particle' is not imaged every 3 or 6 days, a time step uncertainty is imparted that particularly affects new ice and ridged ice production. In fact, a time gap of more than 15 days requires that a grid cell be stopped and not propagated or reinitialized with a new grid cell at a later time.

The characteristics of the ENVISAT ASAR wide swath image mode provide excellent compatibility with the RGPS input image requirements, including frequency and resolution. The 400 km swath enables nearly 100% mapping of the Arctic basin every 3-days or 12 mappings every 35-day orbit repeat cycle. Several key calibration parameters will be improvements on the RADARSAT data quality and should likewise improve the RGPS output quality. These include absolute location accuracy down to 2 pixels (150 m) and radiometric error of 0.2 dB. Also, the availability of strip map data will reduce data manipulation requirements within the RGPS. The RGPS would ingest ASAR Level 1 image data and make the output products globally available. With dedicated and long-term mappings, this Arctic data would continue the monitoring of the climatic changes of the Arctic sea ice cover. Lastly, another key consideration is for development of similar products for the Antarctic sea ice cover, which at minimum would require an increase in SAR data acquisitions over key selected regions.

Recently, the ADEOS-2 spacecraft was lost which carried onboard two critical polar instruments, AMSR and SeaWinds-2, the follow-ons to SSMI and QuikScat, respectively. While

currently there are no gaps in these equivalent sensors, as the long-running SSMI on the DMSP and AMSR-E on NASA's Terra mission, and NASA's QuikScat/SeaWinds-1 are all fully operational, the increased temporal coverage for both the PM and scatterometers was likely to be of exceptional scientific value. QuikScat is already operating beyond its designed lifetime, and as a SeaWinds replacement will take a few years to launch, there could exist in the future a gap in scatterometer measurements if QuikScat fails. Both types of sensors are needed so that the time series of ice extent, seasonal melt, and the more recently developed identification of the perennial and seasonal ice zones continues. Also it is clear that the synergistic use of both types of sensors will lead to improvements in each of these measurements.

The measurement of ice thickness from space has proven elusive until the recent publication of results using ERS-1/-2 altimeters (Laxon et al., 2003). These measurements will be improved in the future, as the Envisat altimeter has increased accuracy in vertical resolution and waveform tracking compared to ERS, Cryosat will measure topography within a 10+ km wide nadir swath which enables the acquisition of a complete map of the sea ice cover over a shorter time interval than previous altimeters. ICESAT has finer horizontal resolution than any of the radar altimeter missions, but snow thickness and cloud cover impact the laser altimeter measurement accuracy. Of key value for observing sea ice thickness as a climate indicator would be increased knowledge of the synoptic-scale ice thickness distribution, needed to understand mass volume as well as which portion of the thickness regime might be changing. This knowledge would require even further improvements in height accuracy for freeboard measurements than are currently planned and novel concepts that would enable the direct measurement of the ice thickness volume. The legacy of sea ice measurements initiated with Seasat is extensive, but the most critical sea ice measurement, ice thickness, awaits continued improvement and instrument capabilities.

4. REFERENCES

Agnew, L., H. Le, and T. Hirose, Estimation of large-scale sea ice motion from SSM/I 85.5 GHz imagery, *Ann. Glaciol.*, 25, 305-311, 1997.

Bertoia, C., J. Falkingham, and F. Fetterer, Polar SAR data for operational sea ice mapping, in R. Kwok and C. Tsatsoulis (Eds.), *Recent Advances in the Analysis of SAR Data of the Polar Oceans*, Springer Verlag, 201-234, 1998.

Bjork, G, J. Soderkvist, P. Winsor, A. Nikolopoulos A., and M. Steele, Return of the cold halocline layer to the Amundsen Basin of the Arctic Ocean: Implications for the sea ice mass balance, *Geophys. Res. Lett.*, 29 (11): art. no. 1513, 2002.

Carsey, F. D., Summer Arctic sea ice character from satellite microwave data, *J. Geophys. Res.*, 90(C3), 5015-5034, 1985.

Carsey, F., and B. Holt, Beaufort-Chukchi ice margin data from Seasat - Ice motion, *J. Geophys. Res.*, 92 (C7), 7163-7172, 1987.

Carsey, F. and G. Pihos, Beaufort-Chukchi ice margin data from Seasat for ice conditions analogous to those of the Labrador Sea, *IEEE Trans. Geosci. Remote Sens.*, 27, 41–551, 1989.

Comiso, J., and R. Kwok, Surface and radiative characteristics of the summer Arctic sea ice cover from multisensor satellite observations, *J. Geophys. Res.*, 101(C12), 28,397-28,416, 1996.

Comiso, J., A rapidly declining perennial sea ice cover in the Arctic, *Geophys. Res. Lett.*, 29 (20), 1956, 2002GL015650, 2002.

Curlander, J. C., B. Holt, and K. J. Hussey, Determination of sea ice motion using digital SAR imagery, *IEEE J. Oceanic Eng., OE-10 (4)*, 358-367, 1985.

Drinkwater, M. R., and X. Liu, Seasonal to interannual variability in Antarctic sea-ice surface melt, *IEEE Trans. Geosci. Remote Sens.*, 38(4), 1827-1842, 2000.

Drobot, S., and M. A. Anderson, An improved method for determining snowmelt onset dates over Arctic sea ice using scanning multichannel microwave radiometer and Special Sensor Microwave/Imager data, *J. Geophys. Res.*, 106(D20), 24,033-24,049, 2001.

Emery, W. J., C. W. Fowler, and J. A. Maslanik, Satellite-derived maps of Arctic and Antarctic sea ice motion, 1988-1994, *Geophys. Res. Lett.*, 24(8), 897-900, 1997.

Evans, D., W. Alpers, A. Cazenave C. Elachi, T. Farr, D. Glackin, B. Holt, L. Jones, W. T. Liu, W.McCandless, Y. Menard, R. Moore, and E. Njoku, Seasat-A 25 year legacy of success, *IEEE Trans. Geosci. Remote Sens.*, submitted 2003.

Fetterer, F. M., D. Gineris, and R. Kwok, Sea ice type maps from Alaska Synthetic Aperture Radar Facility imagery: An assessment, *J. Geophys. Res.*, 99(C11), 22,443-22,458, 1994.

Fily, M., and D. A. Rothrock, Sea ice tracking by nested correlations, *IEEE. Trans. Geosci. Remote Sens.*, GE-25(5), 570-580, 1987.

Forster, R. R., D. G. Long, K. C. Jezek, S. D. Drobot, and M. R. Anderson, The onset of Arctic sea-ice snowmelt as detected with passive- and active-microwave remote sensing, *Ann. Glaciol.*, 33, 85-93, 2001.

Hall, R. T., and D. A. Rothrock, Sea ice displacement from Seasat synthetic aperture radar, *J. Geophys. Res., 86 (C11)*, 11,078-11,082, 1981.

Hibler, W. D., Modelling the formation and evolution of oriented fractures in sea ice, *Annal. Glaciology*, 33: 157-164, 2001.

Kattenberg, A., F. Giorgi, H. Grassl, G. A. Meehl, J. F. B. Mitchell, R. J. Stouffer, T. Tokioka, A. J. Weaver, and T. M. L. Wigley, Climate models: Projections of Future Climate, in J. T. Houghton, L. G. Miera Filho, B. A. Callander, N. Harris, A. Kattenberg, and K. Maskell, eds., *Climate Change 1995*, Cambridge, 285-357, 1996.

Kovacs, A., and R. M. Morey, Electromagnetic measurements of multi-year sea ice using impulse radar, *Cold Regions Sci. Tech.*, 12, 67-93, 1986.

Kwok, R. The RADARSAT Geophysical Processor System, in *Analysis of SAR data of the Polar Oceans: Recent Advances*,

Tsatsoulis, C. and R. Kwok, Eds., Springer-Verlag, 235-258, 1998.

Kwok, R., Recent changes in the Arctic Ocean sea ice circulation associated with the NAO, *Geophys. Res. Lett.*, 27 (6), 775-778, 2000.

Kwok, R., and G. F. Cunningham, Seasonal ice area and volume production of the Arctic Ocean: November 1996 through April 1997, *J Geophys. Res.*, 107 (C10): art. no. 8038, 2002.

Kwok, R., G. F. Cunningham, and S. Yueh, Area balance of the Arctic Ocean perennial ice zone: October 1996 to April 1997, *J. Geophys. Res.*, 104 (C11), 25747-25759, 1999.

Kwok, R.,A. Schweiger, D. A. Rothrock, S. Pang, and C. Kottmeier, Sea ice motion from satellite passive microwave imagery assessed with ERS SAR and buoy motions, *J. Geophys. Res.*,103(C4), 8191-8214, 1998.

Kwok, R., J. C. Curlander, R. McConnell, and S. S. Pang, An ice-motion tracking system at the Alaska SAR Facility, *IEEE J Oceanic Eng.*, 15(1), 44-54, 1990.

Kwok, R., E. Rignot, B. Holt, and R. Onstott, Identification of sea ice types in spaceborne synthetic aperture radar data, *J Geophys. Res.*, 97 (C2), 2391-2402, 1992.

Kwok, R. and D. A. Rothrock, Variability of Fram Strait Flux and North Atlantic Oscillation, *J. Geophys. Res.*, 104(C3), 5177-5189, 1999.

Kwok, R., D. A. Rothrock, H. L. Stern, and G. F. Cunningham, Determination of ice age using lagrangian observations of ice motion, *IEEE Trans. Gesoci Remote Sens.*, 33(2), 392-400, 1995.

Laxon, S. W., Sea ice altimeter processing scheme at the EODC, *Int. J. Remote Sens.*, 15 (4), 915-924, 1994.

Laxon S., Peacock N., and Smith D., High interannual variability of sea ice thickness in the Arctic region, *Nature*, 425 (6961), 947-950, 2003.

Lindsay, R. W., and H. L. Stern, The RADARSAT geophysical processor system: Quality of sea ice trajectory and deformation estimates, *J. Atmos. Oceanic Tech.*, 20 (9), 1333-1347, 2003.

Liu, A. and D. J. Cavalieri, On sea ice drift from the wavelet analysis of DMSP SSM/I data, *Int. J. Remote Sens.*, 19(7), 1415-1423, 1998.

Liu, A., Y. Zhao, and S. Y. Wu, Arctic sea ice drift from wavelet analysis of NSCAT and SSM/I data, *J. Geophys. Res.*, 104(C5), 11529-11538, 1999.

Martin, T. and E. Augstein, Large-scale drift of Arctic sea ice retrieved from passive microwave satellite data, *J. Geophy. Res.*, 105(C4), 8775-8788, 2000.

Parkinson, C. L., and D. J. Cavalieri, A 21 year record of Arctic sea-ice extents and their regional, seasonal and monthly variability and trends, *Ann. Glaciol.*, 34, 441-446, 2002.

Parmerter, R. R., and M. Coon, Model of pressure ridge formation in sea ice, *J. Geophys. Res.*, 77, 6565-6575, 1972.

Peacock, N.R., S.W. Laxon, W. Maslowski, D.P. Winebrenner, and R.J. Arthern, Geophysical signatures from precise altimetric height measurements in the Arctic Ocean, paper presented at IGARSS '98, Seattle, WA, USA, edited T.I. Stein, 1964-1966, IEEE, 1998.

Proshutinsky, A. Y., and M. A. Johnson, Two circulation regimes of the wind-driven Arctic Ocean, *J. Geophys. Res.*, 102, 12,493-12,514, 1997.

Remund, Q. P., D. G. Long, and M. R. Drinkwater, An iterative approach to multisensor sea ice classification, *IEEE Trans. Geosci. Remote Sens.*, 38 (4): 1843-1856 Part 2, 2000.

Richter-Menge, J. A., S. L. McNutt, J. E. Overland, and R. Kwok, Relating arctic pack ice stress and deformation under winter conditions, *J. Geophys. Res.*, 107(C10), 8040, doi:10.1029/2000JC000477, 2002.

Rothrock, D. A., Y. Yu, and G. A. Maykut, Thinning of the Arctic sea-ice cover, *Geophys. Res., Lett.*, 26(23), 3469-3472, 1999.

Rothrock, D. A., J. Zhang, and Y. Yu, The arctic ice thickness anomaly of the 1990s: A consistent view from observations and models, *J. Geophys. Res.*, 108(C3), art. no. 3083, 2003.

Smith, D. A., Recent increase in the length of the melt season of perennial Arctic sea ice, *Geophys. Res. Lett.*, 25(5), 655-658, 1998.

Steele, M., and T. Boyd,, Retreat of the cold halocline layer in the Arctic Ocean, *J. Geophys. Res.*, 103(C5), 10,419-10,435, 1998.

Stern, H. L., D. A. Rothrock, and R. Kwok, Open water production in Arctic sea-ice – Satellite measurements and model parameterizations, *J. Geophys. Res.*, 100 (C10), 20601-20612, 1995.

Ulander, L. M. H., Interpretation of Seasat radar-altimeter data over sea ice using near-simultaneous SAR imagery, *Inter. J. Remote Sens.*, 8(11), 1679-1686, 1987.

U. S. National Research Council, *Enhancing NASA's contributions to polar science,* National Academy Press, Washington DC, 124 pp., 2001.

Winebrenner, D. P., D. G. Long, and B. Holt, Mapping the progression of melt onset and freeze-up on Arctic sea ice using SAR and scatterometry, in C. Tsatsoulis and R. Kwok (eds), *Analysis of SAR Data in the Polar Oceans*, Springer-Verlag, 129-144, 1998.

Wingham, D.J., A.J. Ridout, R. Scharroo, R.J. Arthern and C.K. Shum, Antarctic elevation change 1992 to 1996, *Science*, 282, 456-458, 1998.

Wingham, D., The first of the European Space Agency's opportunity missions: CryoSat, *Earth Observation Quarterly*, 63, ESA, 1999.

Yueh S.H., R. Kwok, S-H. Lou, and W.-Y. Tsai, Sea ice identification using dual-polarized Ku-band scatterometer data, *IEEE Trans. Geosci. Remote Sens.*, 35 (3), 560-569, 1997.

Zhang, J., D. Rothrock, and M. Steele, Recent changes in Arctic sea ice: The interplay between ice dynamics and thermodynamics, *J. Climate,* 13, 3099-3114, 2000.

Zhang, J. L., D. R. Thomas, D. A. Rothrock, R. W. Lindsay, Y. Yu, and R. Kwok, Assimilation of ice motion observations and comparisons with submarine ice thickness data, *J. Geophys. Res.*, 108 (C6): art. no. 3170, 2003

Zwally, H. J., M. A. Beckley, A. C. Brenner, and M. B. Giovinetto, Motion of major ice-shelf fronts in Antarctica from slant-range analysis of radar altimeter data, 1978-98, *Annal. Glaciol.*, 34, 255-262, 2002B.

Zwally, H. J., J. C. Comiso, C. L. Parkinson, D. J. Cavalieri, and P. Gloersen, Variability of Antarctic sea ice 1979-1998, *J Geophys. Res.*, 107(C5), art. no. 3041, 2002A.

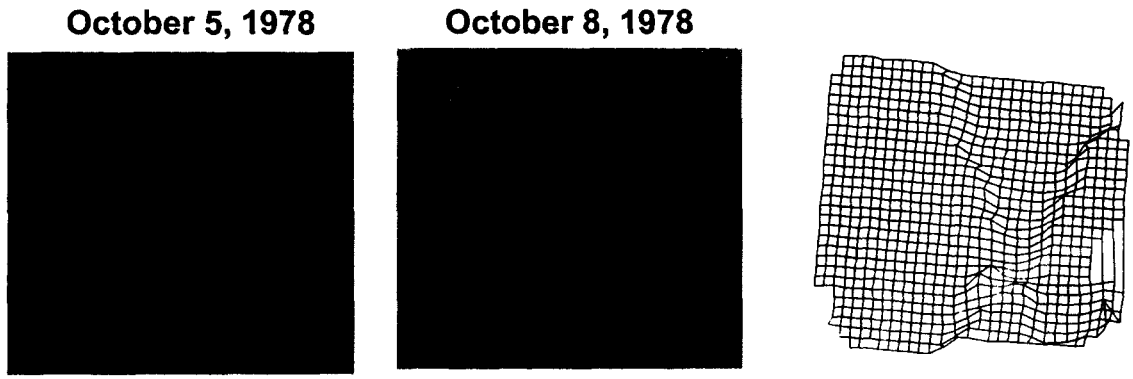

Figure 1. Seasat SAR image pair of sea ice in the Beaufort Sea taken 3 days apart. Each image is 100 by 100 km. The grid shows areas that have deformed and aggregated floes that have moved as rigid pieces. (After Fily and Rothrock, 1987).

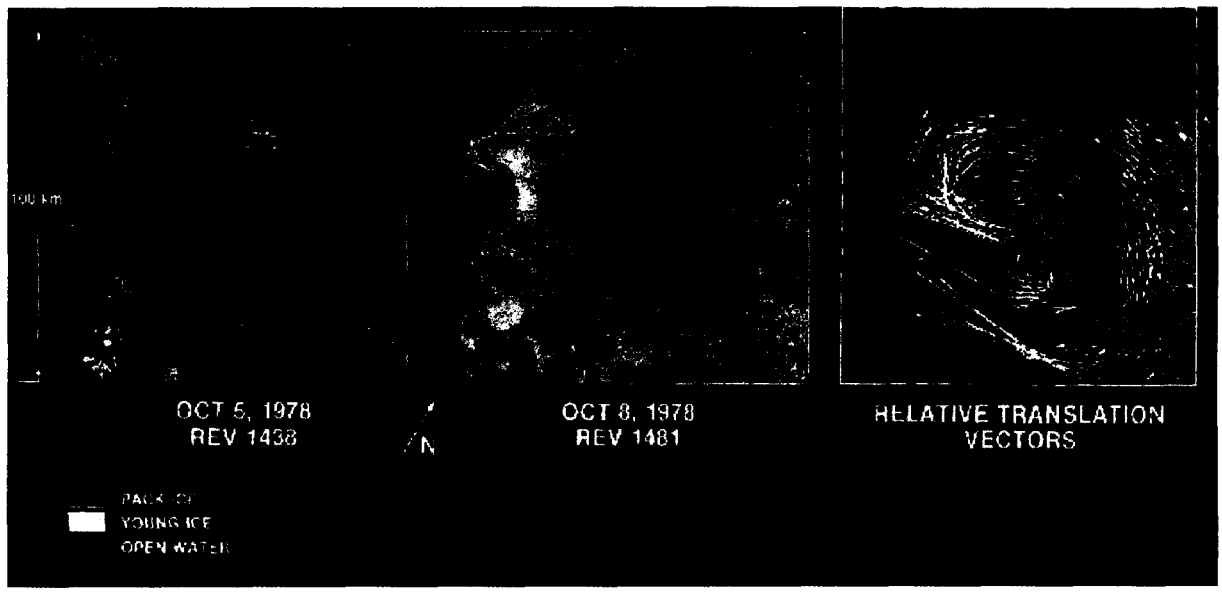

Figure 2. Seasat SAR image pair of sea ice at the Chukchi Sea ice margin, that also shows ice type classification. The third panel indicates that an ocean eddy has caused the ice field to rotate and form an open water area. (After Carsey and Holt, 1987).

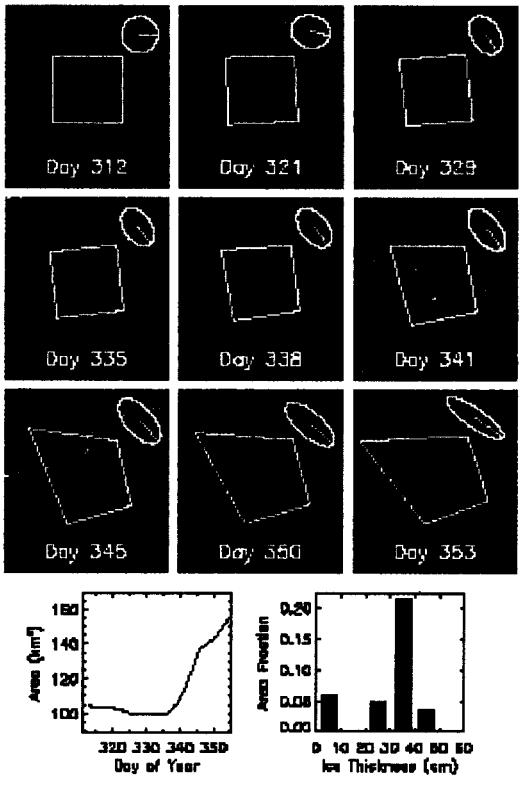

Figure 3. The deformation of a 10 km by 10 km cell over a 41-day period is shown from RADARSAT. The record of area change reflects the opening of the lead running through the cell. The strain ellipses are computed from strain rates.

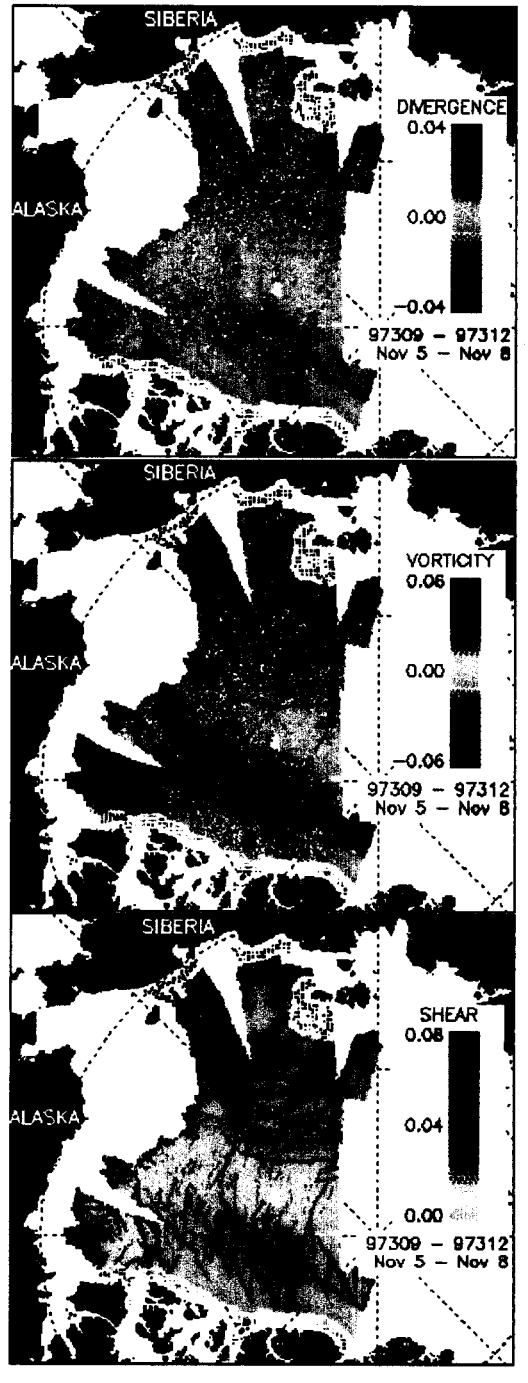

Figure 4. The deformation of the ice cover over three days between Day 309 and 312 in 1997 derived from RADARSAT data by the RGPS. (a) Divergence. (b) Vorticity. (c) Shear.

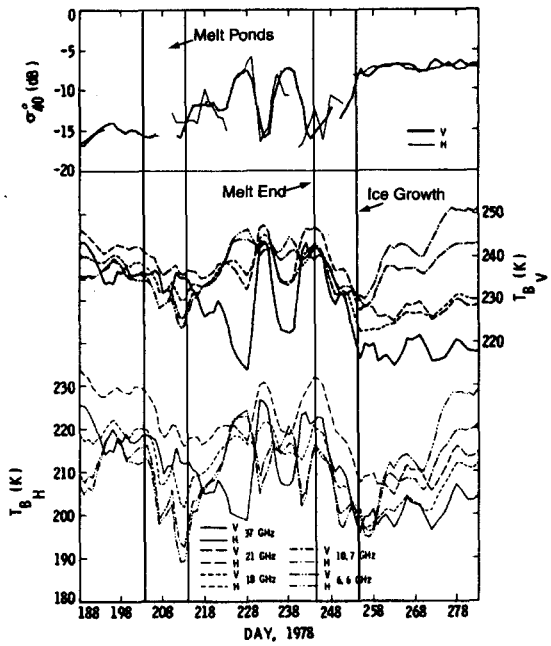

Figure 5. The seasonal cycle of sea ice melt in the Beaufort Sea detected by the Seasat SASS (top panel) and SMMR (bottom panel) in 1978. Melt onset and freeze-up occurs on about day 204 and day 245, respectively. Also indicated are the formation of melt ponds and the beginning of ice growth. (After Carsey, 1985).

Figure 6. Gridded (100 km) estimates of ice thickness derived from altimeter measurements of freeboard from the ERS-2 radar altimeter. (Figure courtesy of S. Laxon).